Available online at www.sciencedirect.com
ScienceDirect
Journal of Computational Physics 226 (2007) 263–281
JOURNAL OF COMPUTATIONAL PHYSICS
www.elsevier.com/locate/jcp

Adapted polynomial chaos expansion for failure detection

M. Paffrath *, U. Wever [1]

Siemens AG, Corporate Technology, Otto-Hahn-Ring 6, D81730 Munich, Germany

Received 23 May 2006; received in revised form 30 March 2007; accepted 9 April 2007
Available online 24 April 2007

Abstract

In this paper, we consider two methods of computation of failure probabilities by adapted polynomial chaos expansions. The performance of the two methods is demonstrated by a predator–prey model and a chemical reaction problem.

MSC: 41A10; 60Gxx; 65C30; 92D25; 92E20

Keywords: Polynomial chaos; Stochastic differential equations; Stochastic processes; Probability of failure

1. Introduction

Failure detection for systems with uncertainties is an ongoing topic in literature. Many concepts have already been introduced. Among the most established methods are FORM and SORM which are based on a Taylor approximation of the failure function in the point of highest failure probability, see [1,8,9,11,17]. For problems with mild nonlinearities, FORM and SORM are very fast and accurate methods. However, for high nonlinearities, the resolution of these methods may not be sufficient, and more accurate and therefore more expensive methods are required. Furthermore, FORM and SORM require derivative information which is not always available. Among the methods that do not require derivative information are advanced Monte Carlo methods, see [16].

In recent years, polynomial chaos expansion has become a very powerful tool for treating uncertainties, see [10]. The method is especially well suited for complex systems such as finite element analysis and computational fluid dynamics, see [19]. In [4] stochastic finite element analysis has been established on the basis of Hermite-chaos expansion. This fundamental work has been later extended to a generalized, Askey-scheme based, polynomial chaos expansion gPC [26]. In [23,24] multi-element generalized polynomial chaos expansion of the random space (ME-gPC) is introduced in order to increase the effectiveness of gPC. This decomposition corresponds to a *h*-type refinement of the random space. In [12,13] the random space is decomposed using

* Corresponding author. Tel.: +49 89 636 41117; fax: +49 89 636 45111.
E-mail addresses: meinhard.paffrath@siemens.com (M. Paffrath), utz.wever@siemens.com (U. Wever).
[1] Tel.: +49 89 636 46103; fax: +49 89 636 45111.

0021-9991/$ - see front matter
doi:10.1016/j.jcp.2007.04.011

wavelets. So effective and accurate methods exist for the computation of central moments of the output, such as the mean or the variance. For failure detection, information is required far away from the mean of the input, in regions at the boundary of the input cumulative density function, because the mean of the input itself should be of course in the safe region. The common polynomial chaos expansion, which may be interpreted as an expansion about the mean of the stochastic process, is not suitable for reliability analysis at high sigma level (say larger than five sigma). Some concepts to overcome this problem have already been introduced. Ghanem proposes using additional sample information in the orthogonal complement of the Hermite expansion, see [4–6].

In this paper, we concentrate on most probable-point-based methods where the problem of computation of the failure probability splits into two parts: *identifying* and *resolving* the failure region. We present two polynomial chaos expansions which are suitable for *resolving* the failure region which we call shifted (SH) and windowed Hermite expansions (WH). Both methods aim at zooming into the critical region. The shifted Hermite expansion is simply a Hermite expansion with respect to a shifted mean of the input. The windowed Hermite expansion is a restriction of the normal Hermite expansion to a subset of the random space. Its construction is analogous to the construction of one smaller element of the random space decomposition in [23,24] whose work we learned of after finishing this paper. For *identifying* the failure region we can, for instance, compute the point of highest failure probability ('Beta point') as is done in the FORM method. For evaluation of the failure integral, we apply a sampling method to the Hermite approximation. We are mainly interested in problems with, in terms of CPU time, very expensive function evaluations (for example CFD problems). In these problems sampling of the Hermite approximation is not prohibitive because the cost of evaluation and even sampling of the Hermite approximation is much cheaper than the cost of one function evaluation. We show that the proposed methods provide the desired failure information with higher accuracy than the usual (central) Hermite expansion, with no higher computational complexity. Both methods are not restricted to failure analysis, but generally provide a higher resolution of the solution in subdomains. In particular, the proposed methods can be applied to stochastic finite elements. In this paper, we restrict ourselves to applications from the field of stochastic ordinary differential equations. The first example is a predator–prey model where the probability of survival of the two species is computed. The second one is an oscillating chemical reaction problem. The probability is computed that the amplitude of one species falls below a given limit. In the presented examples, exact computation of the point of highest failure probability for identifying the failure region is not necessary.

2. Central Hermite chaos (CH)

According to Wiener [25], homogeneous chaos is defined as a span of Hermite polynomial functional of a Gaussian process. The theorem of Cameron and Martin [2] implies that the Fourier–Hermite series can approximate any functional in L_2 and converges in the L_2 sense. So second-order random processes can be expanded in terms of orthonormal Hermite polynomials. A general second order random process $x(\Theta)$, with Θ being the random event, can be represented in the form:

$$x(\Theta) = a_0 H_0 + \sum_{i_1=1}^{\infty} a_{i_1} H_1(\xi_{i_1}(\Theta)) + \sum_{i_1=1}^{\infty} \sum_{i_2=1}^{i_1} a_{i_1 i_2} H_2(\xi_{i_1}(\Theta), \xi_{i_2}(\Theta)) + \sum_{i_1=1}^{\infty} \sum_{i_2=1}^{i_1} \sum_{i_3=1}^{i_2} a_{i_1 i_2 i_3} H_3(\xi_{i_1}(\Theta), \xi_{i_2}(\Theta), \xi_{i_3}(\Theta)) + \cdots, \tag{1}$$

where $H_j(\xi_{i_1}(\Theta), \ldots, \xi_{i_j}(\Theta))$ denotes the Hermite chaos of order j in the variables $(\xi_{i_1}, \ldots, \xi_{i_j})$ and the H_j are Hermite polynomials in terms of the standard Gaussian variables $\boldsymbol{\xi}$ with zero mean and unit variance. The H_j are generated by the formula of Rodriguez:

$$H_j(\boldsymbol{\xi}) = (-1)^j \mathrm{e}^{\frac{1}{2}\boldsymbol{\xi}^{\mathrm{T}}\boldsymbol{\xi}} \frac{\partial^j}{\partial \xi_{i_1} \cdots \partial \xi_{i_j}} \mathrm{e}^{-\frac{1}{2}\boldsymbol{\xi}^{\mathrm{T}}\boldsymbol{\xi}}. \tag{2}$$

In one dimension, the first three polynomials are:

$$H_0(\xi) = 1, \tag{3}$$
$$H_1(\xi) = \xi, \tag{4}$$
$$H_2(\xi) = \xi^2 - 1. \tag{5}$$

Eq. (1) can be rewritten, for notational convenience, in the form

$$x(\Theta) = \sum_{i=0}^{\infty} \hat{a}_i \Psi_i(\boldsymbol{\xi}), \tag{6}$$

where there is a one-to-one correspondence between the functions $H_j(\xi_{i_1}, \ldots, \xi_{i_j})$ and $\Psi_i(\boldsymbol{\xi})$. The polynomials Ψ_i form a complete orthonormal basis of the Hilbert space H with the inner product:

$$\langle f(\boldsymbol{\xi}), g(\boldsymbol{\xi}) \rangle = \frac{1}{\sqrt{(2\pi)^n}} \int_{\mathbb{R}^n} f(\boldsymbol{\xi}) g(\boldsymbol{\xi}) \mathrm{e}^{\frac{1}{2}\boldsymbol{\xi}^{\mathrm{T}}\boldsymbol{\xi}} \, \mathrm{d}\boldsymbol{\xi}. \tag{7}$$

So

$$H = \mathrm{span}\{\Psi_0(\boldsymbol{\xi}), \Psi_1(\boldsymbol{\xi}), \Psi_3(\boldsymbol{\xi}), \ldots\} \tag{8}$$

see also [19].

Thus, each functional $f(\boldsymbol{\xi}(\Theta)) \in H$ with

$$\langle f(\boldsymbol{\xi}(\Theta)), f(\boldsymbol{\xi}(\Theta)) \rangle < \infty$$

may be approximated by a series of Hermite polynomials in the L_2 sense:

$$f(\Theta) = \sum_{i=0}^{\infty} c_i \Psi_i(\boldsymbol{\xi}(\Theta)). \tag{9}$$

Best approximation of a function $f(\boldsymbol{\xi})$ in the Hermite base

$$\min_{c \in \mathbb{R}^n} \| f(\boldsymbol{\xi}) - \sum_{i=0}^{M} c_i \Psi_i(\boldsymbol{\xi}) \|^2 \tag{10}$$

leads to the normal equations:

$$\left\langle \left(f(\boldsymbol{\xi}) - \sum_{i=0}^{M} c_i \Psi_i(\boldsymbol{\xi}) \right), \ \Psi_k(\boldsymbol{\xi}) \right\rangle = 0, \quad k = 0, \ldots, M. \tag{11}$$

Due to the orthonormality of the base functions, Eq. (11) reduces to the common Fourier integrals:

$$c_i = \langle f(\boldsymbol{\xi}), \Psi_i(\boldsymbol{\xi}) \rangle = \frac{1}{\sqrt{(2\pi)^n}} \int_{\mathbb{R}^n} f(\boldsymbol{\xi}) \Psi_i(\boldsymbol{\xi}) \mathrm{e}^{-\frac{1}{2}\boldsymbol{\xi}^{\mathrm{T}}\boldsymbol{\xi}} \, \mathrm{d}\boldsymbol{\xi}, \quad i = 0, \ldots, M, \tag{12}$$

where c_0 is the mean of $f(\boldsymbol{\xi})$.

The coefficients (12) may be computed by a multi-dimensional Gauss–Hermite quadrature [3]:

$$c_i \approx \sum_{j=1}^{N} w_j f(\boldsymbol{\xi}^j) \Psi_i(\boldsymbol{\xi}^j), \quad i = 0, \ldots, M \tag{13}$$

with multi-weights w_j and abscissae $\boldsymbol{\xi}^j$, $j = 1, \ldots, N$. The components ξ_k^j of $\boldsymbol{\xi}^j$ are the roots of the one-dimensional basic polynomial H_s of degree s and

$$N = s^n. \tag{14}$$

In [7], we have developed an adaptive, error controlled Gauss quadrature, which is especially well suited for high dimensions n. With this algorithm, the number N of function evaluations of the non-adaptive Gauss quadrature may be reduced drastically.

Also time dependent Gaussian processes, which are described by a differential equation, may be approximated by a series of Hermite polynomials. Let

$$y(t,\xi) \approx \sum_{i=0}^{M} y_i(t)\Psi_i(\xi), \quad \dot{y}(t,\xi) = f(y(t,\xi),\xi). \tag{15}$$

Inserting the series into the differential equation and projecting the resulting equation onto the Hermite base leads to the following equations:

$$\sum_{i=0}^{M} \dot{y}_i(t)\langle \Psi_i(\xi), \Psi_k(\xi)\rangle = \left\langle f\left(\sum_{i=0}^{M} y_i(t)\Psi_i(\xi)\right),\ \Psi_k(\xi)\right\rangle, \quad k = 0,\ldots,M. \tag{16}$$

Due to the orthonormality of the base functions, it holds:

$$\dot{y}_k(t) = \left\langle f\left(\sum_{i=0}^{M} y_i(t)\Psi_i(\xi)\right),\ \Psi_k(\xi)\right\rangle, \quad k = 0,\ldots,M. \tag{17}$$

3. Shifted Hermite chaos (SH)

Shifted Hermite chaos is a special most probable-point-based method for evaluation of failure probabilities. Let the failure function be given by

$$g(\xi)\begin{cases} \geqslant 0 & \text{stable,} \\ < 0 & \text{not stable.} \end{cases} \tag{18}$$

Then the probability of failure is

$$P(g(\xi) \leqslant 0) = \int_{g(\xi)\leqslant 0} \rho_\xi(\xi)\, \mathrm{d}\xi, \tag{19}$$

where $\rho_\xi(\xi)$ is the density of the random variable ξ.

For failure detection, a good resolution of the region of large failure probability is necessary. For standard normal random variables, the point of the largest probability of failure ('Beta point') is usually calculated as the solution of the optimization problem [17]:

$$\min \|\xi\|^2, \quad g(\xi) \leqslant 0. \tag{20}$$

By 'shifted' Hermite chaos (SH) we simply mean the normal Hermite chaos with respect to a shifted mean $\boldsymbol{\mu}$ of the input. $\boldsymbol{\mu}$ may be the Beta point or an approximation of it. Though there is no theoretical difference between (SH) and (CH), we would like to make some short comments on it. A stochastic function may be written as:

$$f(\xi + \boldsymbol{\mu}) = \sum_{i=0}^{\infty} c_i \Psi_i(\xi) \tag{21}$$

or

$$f(\tilde{\xi}) = \sum_{i=0}^{\infty} c_i \Psi_i(\tilde{\xi} - \boldsymbol{\mu}) = \sum_{i=0}^{\infty} c_i \Psi_i^s(\tilde{\xi}), \tag{22}$$

where $\tilde{\xi}$ is now a random vector with mean value $\boldsymbol{\mu}$. With respect to the following inner product, the shifted Hermite polynomials form an orthonormal basis:

$$\langle f(\tilde{\xi}), g(\tilde{\xi})\rangle_s = \frac{1}{\sqrt{(2\pi)^n}} = \int_{\mathbb{R}^n} f(\tilde{\xi}) g(\tilde{\xi}) \mathrm{e}^{-\frac{1}{2}(\tilde{\xi}-\boldsymbol{\mu})^{\mathrm{T}}(\tilde{\xi}-\boldsymbol{\mu})}\, \mathrm{d}\tilde{\xi} \tag{23}$$

The projection of the shifted Hermite chaos (21) onto the centralized base functions (2) and truncation of the series leads to a linear system for the unknown coefficients $U_i(t)$:

$$\langle f(\xi + \boldsymbol{\mu}), \Psi_k(\xi)\rangle = \sum_{i=0}^{M} c_i \langle \Psi_i(\xi), \Psi_k(\xi)\rangle, \quad k = 0,\ldots,M. \tag{24}$$

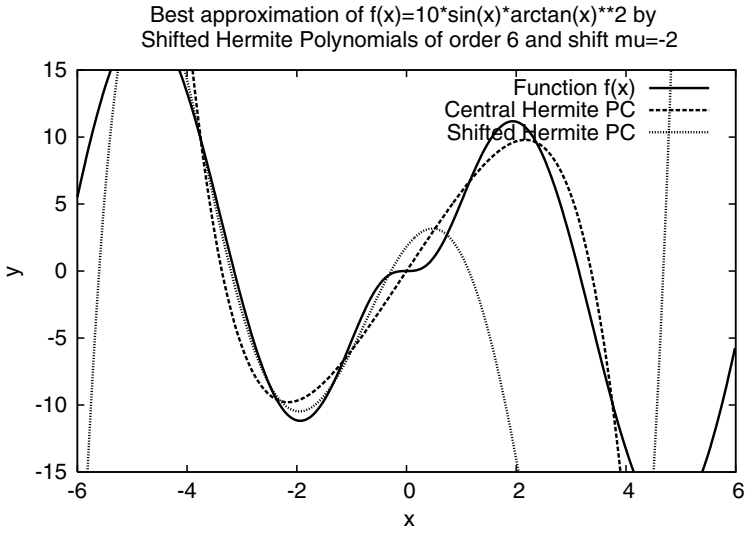

Fig. 1. Best approximation of the function $f(x) = 10 * \sin(x) * \arctan(x) ** 2$ in the range $[-6:6]$ by shifted Hermite polynomials. It holds $\boldsymbol{\mu} = -2$.

Eq. (24) may be interpreted as a best approximation of a function $f(\Theta)$ by Hermite approximation in the shifted scalar product (23):

$$
\begin{aligned}
0 &= \langle f(\boldsymbol{\xi}+\boldsymbol{\mu}), \Psi_k(\boldsymbol{\xi})\rangle - \sum_{i=0}^{M} c_i \langle \Psi_i(\boldsymbol{\xi}), \Psi_k(\boldsymbol{\xi})\rangle = \left\langle f(\boldsymbol{\xi}+\boldsymbol{\mu}) - \sum_{i=0}^{M} c_i \Psi_i(\boldsymbol{\xi}), \Psi_k(\boldsymbol{\xi}) \right\rangle \\
&= \frac{1}{\sqrt{(2\pi)^n}} \int_{\mathbb{R}^n} \left[f(\boldsymbol{\xi}+\boldsymbol{\mu}) - \sum_{i=0}^{M} c_i \Psi_i(\boldsymbol{\xi}) \right] \Psi_k(\boldsymbol{\xi}) \mathrm{e}^{-\frac{1}{2}\boldsymbol{\xi}^{\mathrm{T}}\boldsymbol{\xi}} \, \mathrm{d}\boldsymbol{\xi} \\
&= \frac{1}{\sqrt{(2\pi)^n}} \int_{\mathbb{R}^n} \left[f(\tilde{\boldsymbol{\xi}}) - \sum_{i=0}^{M} c_i \Psi_i^s(\tilde{\boldsymbol{\xi}}) \right] \Psi_k^s(\tilde{\boldsymbol{\xi}}) \mathrm{e}^{-\frac{1}{2}(\tilde{\boldsymbol{\xi}}-\boldsymbol{\mu})^{\mathrm{T}}(\tilde{\boldsymbol{\xi}}-\boldsymbol{\mu})} \, \mathrm{d}\tilde{\boldsymbol{\xi}} = \left\langle f(\tilde{\boldsymbol{\xi}}) - \sum_{i=0}^{M} c_i \Psi_i^s(\tilde{\boldsymbol{\xi}}), \Psi_k^s(\tilde{\boldsymbol{\xi}}) \right\rangle_s .
\end{aligned}
$$

The corresponding best approximation problem is:

$$
\min_{c \in \mathbb{R}^n} \| f(\tilde{\boldsymbol{\xi}}) - \sum_{i=0}^{M} c_i \Psi_i^s(\tilde{\boldsymbol{\xi}}) \|_s^2, \tag{25}
$$

where

$$
\|f\|_s^2 = \langle f, f \rangle_s . \tag{26}
$$

Method (SH) is tested by best approximation of the function

$$
f(x) = 10 * \sin(x) * \arctan(x) * *2, \tag{27}
$$

see Fig. 1.

In the vicinity of shift -2, (SH) approximates the given function more accurately than (CH). As in the centralized case, also stochastic processes given by a differential equation, see Eq. (15), may be handled by the shifted polynomial chaos.

4. Windowed Hermite chaos (WH)

For evaluation of the probability of failure (19) it is essential to have a good approximation of the solution in a neighbourhood $\mathscr{M}$ of the point of highest failure probability (the so called 'Beta' point). One possibility to achieve this goal is to use *conditional* Hermite chaos that is the normal Hermite chaos conditioned on $\mathscr{M}$. The

construction of conditional Hermite chaos is analogous to the construction of smaller elements of the random space decomposition in [23,24]. In 1D, the corresponding scalar product to conditional Hermite chaos is defined by:

$$\langle f, g\rangle = \int_{\mathbb{R}} f(\xi)g(\xi)\rho(\xi|\xi \in \mathscr{M})\,\mathrm{d}\xi$$

with

$$\rho(\xi) = \frac{1}{\sqrt{2\pi}}\mathrm{e}^{-\frac{1}{2}\xi^2}$$

denoting the density of the normal Hermite chaos. For the special case of an interval $\mathscr{M} = [a, b]$ the scalar product is

$$\langle f, g\rangle_w = \int_{\mathbb{R}} f(\xi)g(\xi)\rho(\xi\|a \leqslant \xi \leqslant b)\,\mathrm{d}\xi = \frac{1}{C}\int_a^b f(\xi)g(\xi)\rho(\xi)\,\mathrm{d}\xi$$

with the corresponding norm

$$\|f\|_w = \sqrt{\langle f, f\rangle_w}$$

and

$$C = \int_a^b \rho(\xi)\,\mathrm{d}\xi.$$

This special conditional Hermite chaos will be called *windowed* Hermite chaos (WH) in the following. A set of orthonormal basic polynomials $\{\phi_j,\ j = 1, 2, \ldots\}$ can be constructed by the Gram–Schmidt orthogonalization procedure, see Appendix A. The natural generalization to the n-dimensional case is:

$$\langle f, g\rangle_w = \frac{1}{C}\int_{a_1}^{b_1}\cdots\int_{a_n}^{b_n} f(\boldsymbol{\xi})g(\boldsymbol{\xi})\mathrm{e}^{-\frac{1}{2}\boldsymbol{\xi}^{\mathrm{T}}\boldsymbol{\xi}}\,\mathrm{d}\boldsymbol{\xi} \tag{28}$$

and

$$C = \int_{a_1}^{b_1}\cdots\int_{a_n}^{b_n} \mathrm{e}^{-\frac{1}{2}\boldsymbol{\xi}^{\mathrm{T}}\boldsymbol{\xi}}\,\mathrm{d}\boldsymbol{\xi}.$$

The set $\mathscr{M}$ is now equal to the window $W = [a_1, b_1] \times \cdots \times [a_n, b_n]$ around the Beta point. Analogously to the Hermite polynomials, the n-dimensional basic polynomials for this scalar product can be constructed as tensor products of the one-dimensional polynomials:

$$\Psi_q^w(\boldsymbol{\xi}) = \prod_{k=1}^{n}\phi_{\xi_{qk}}(\xi_k)$$

with multi-indices ξ_q satisfying $\sum_{k=1}^{n}\xi_{qk} \leqslant P$, P is the order of the chaos. An important condition that makes the tensor product construction possible is that in the density function $\rho(\boldsymbol{\xi}) = \mathrm{e}^{-\frac{1}{2}\boldsymbol{\xi}^{\mathrm{T}}\boldsymbol{\xi}}$ coordinates can be separated:

$$\rho(\boldsymbol{\xi}) = \prod_{i}^{n}\rho_i(\xi_i). \tag{29}$$

Condition (29) is fulfilled for independent random variables ξ_i. For dependent normal random variables with covariance matrix $\mathbf{V}$, a linear transformation $\boldsymbol{\xi} = T_L\boldsymbol{\xi}_0$ from $\boldsymbol{\xi}$ to an independent standard normal vector $\boldsymbol{\xi}_0$ may be applied, with T_L given by the Cholesky decomposition of $\mathbf{V}$. For the general case of dependent mixed normal and non-normal random variables, there is no exact transformation available. As approximation, the nonlinear Rosenblatt transformation $\boldsymbol{\xi} = T(\boldsymbol{\xi}_0)$ [18] may be applied. Since the windowed Hermite polynomials form a complete basis in the corresponding Hilbert space, we can expect the windowed Hermite expansion to

converge to any L_2 functional in the L_2 sense in the corresponding Hilbert functional space, as a generalized result of the Cameron–Martin theorem [2]. Best approximation of a function $f(\boldsymbol{\xi})$ in the window W:

$$\min_{c\in\mathbb{R}^n}\left\| f(\boldsymbol{\xi}) - \sum_{i=0}^{M} c_i \Psi_i^w(\boldsymbol{\xi}) \right\|_w^2 \tag{30}$$

leads (see Section 2) to the normal equations:

$$\left\langle \left(f(\boldsymbol{\xi}) - \sum_{i=0}^{M} c_i \Psi_i^w(\boldsymbol{\xi}) \right), \Psi_k^w(\boldsymbol{\xi}) \right\rangle_w = 0, \quad k = 0,\ldots,M \tag{31}$$

with

$$c_i = \langle f(\boldsymbol{\xi}), \Psi_i^w(\boldsymbol{\xi})\rangle_w. \tag{32}$$

As in (13), the coefficients c_i are computed by a multi-dimensional Gauss–Hermite quadrature:

$$c_i \approx \sum_{j=1}^{N} w_j f(\boldsymbol{\xi}^j)\Psi_i^w(\boldsymbol{\xi}^j), \quad i = 0,\ldots,M \tag{33}$$

with multi-weights w_j and abscissae $\boldsymbol{\xi}^j$, $j = 1,\ldots,N$. The components ξ_k^j of $\boldsymbol{\xi}^j$ are the roots of the one-dimensional windowed-Hermite basic polynomial of degree s and $N = s^n$. All roots are distinct and $\xi_k^j \in (a_k, b_k)$ (see [22]), so $\boldsymbol{\xi}^j \in W$, and the Gauss–Hermite quadrature is well defined.

Consider now the two-dimensional example of Fig. 2 where the Beta point is marked by a circle. In order to get a good resolution of g in the neighbourhood of the limit surface $\{\boldsymbol{\xi} : g(\boldsymbol{\xi}) = 0\}$, Fig. 2 shows that it may be advantageous to use a rotated window parallel to the tangent plane in the Beta point. So one coordinate is in the direction of $\nabla g(\boldsymbol{\xi})$ in the Beta point and is closely related to the variation of probability density. There is an orthogonal transformation from the local coordinate system $\boldsymbol{\eta}$ of the rotated window to the original coordinate system $\boldsymbol{\xi}$:

$$\boldsymbol{\xi} = Q\boldsymbol{\eta} + \boldsymbol{\xi}^*,$$

$\boldsymbol{\xi}^*$ is the Beta point, the first column of Q is the normalized gradient $\nabla g(\boldsymbol{\xi})$, the remaining columns can be again computed by Gram–Schmidt, for example.

The scalar product is now

$$\langle f, g\rangle_w = \int_{\alpha_1}^{\beta_1} \cdots \int_{\alpha_n}^{\beta_n} f(\boldsymbol{\eta}) g(\boldsymbol{\eta}) \mathrm{e}^{-\frac{1}{2}(Q\boldsymbol{\eta}+\boldsymbol{\xi}^*)^{\mathrm{T}}(Q\boldsymbol{\eta}+\boldsymbol{\xi}^*)}\, \mathrm{d}\boldsymbol{\eta},$$

where $W_{\mathrm{rot}} = (\alpha_1,\beta_1)\times\cdots\times(\alpha_n,\beta_n)$ is the rotated window. The density function $\rho(\boldsymbol{\eta}) = \mathrm{e}^{-\frac{1}{2}(Q\boldsymbol{\eta}+\boldsymbol{\xi}^*)^{\mathrm{T}}(Q\boldsymbol{\eta}+\boldsymbol{\xi}^*)}$ again fulfills condition (29) due to the orthogonality of Q, so the construction of n-dimensional basic polynomials by

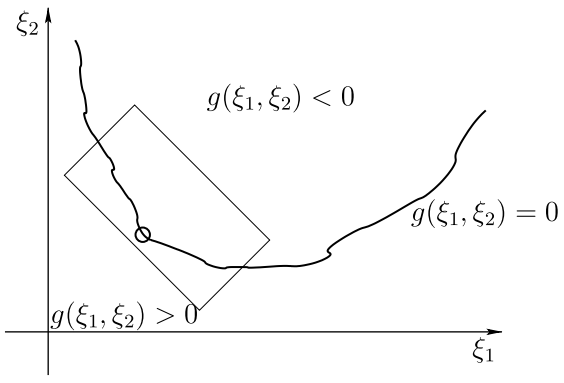

Fig. 2. Rotated window for approximation of g-function.

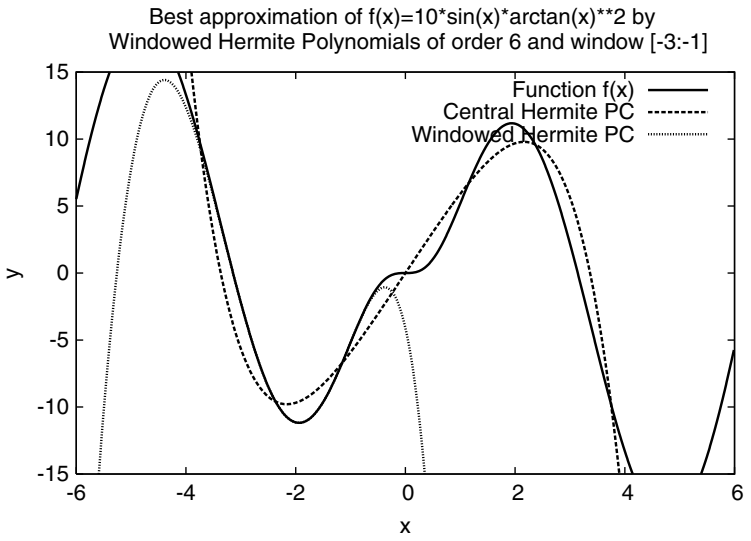

Fig. 3. Best approximation of the function $f(x) = 10 * \sin(x) * \arctan(x) * * 2$ in the range $[-6:6]$ by windowed Hermite polynomials. It holds $[a,b] = [-3,-1]$.

tensor products is possible. Method (WH) is again tested by best approximation of function (27). Fig. 3 shows a comparison with (CH), Fig. 4 shows a comparison with (SH). In the interval $[-3,-1]$, (WH) perfectly fits the given function. So you can see only three curves in Fig. 4.

An error estimation of windowed Hermite chaos for the computation of failure probabilities is given in Appendix B.

5. Probability of failure

In this section, we apply methods (SH) and (WH) to the computation of failure probabilities. Let the failure function and probability of failure be given by (18) and (19), respectively. The solution of the optimization problem (20) defines

- either the shift $\boldsymbol{\mu}$ for the shifted Hermite polynomials $\Psi_i^s(\boldsymbol{\xi})$
- or the center of a window $W = [\mu_1 - c, \mu_1 + c] \times \cdots \times [\mu_n - c, \mu_n + c]$ for the windowed Hermite polynomials $\Psi_i^w(\boldsymbol{\xi})$

Instead of solving the optimization problem, also any other reasonable shift, suggested by the application, may be applied.

The failure function $g(\boldsymbol{\xi})$ is now approximated by one of the modified Hermite expansions:

$$g(\boldsymbol{\xi}) \approx g^m(\boldsymbol{\xi}) = \sum_{i=0}^{M} g_i \Psi_i^m(\boldsymbol{\xi}), \quad m = s, w$$

Often the failure function depends on state variables, which are given by differential equations. Then, the approximation of the failure function is given by

$$g(x_1(\boldsymbol{\xi}), \ldots, x_k(\boldsymbol{\xi})) \approx g^m(\boldsymbol{\xi}) = g\left(\sum_{i=0}^{M} x_{i,1} \Psi_i^m(\boldsymbol{\xi}), \ldots, \sum_{i=0}^{M} x_{i,k} \Psi_i^m(\boldsymbol{\xi})\right), \quad m = s, w.$$

The probability of failure may be now computed by

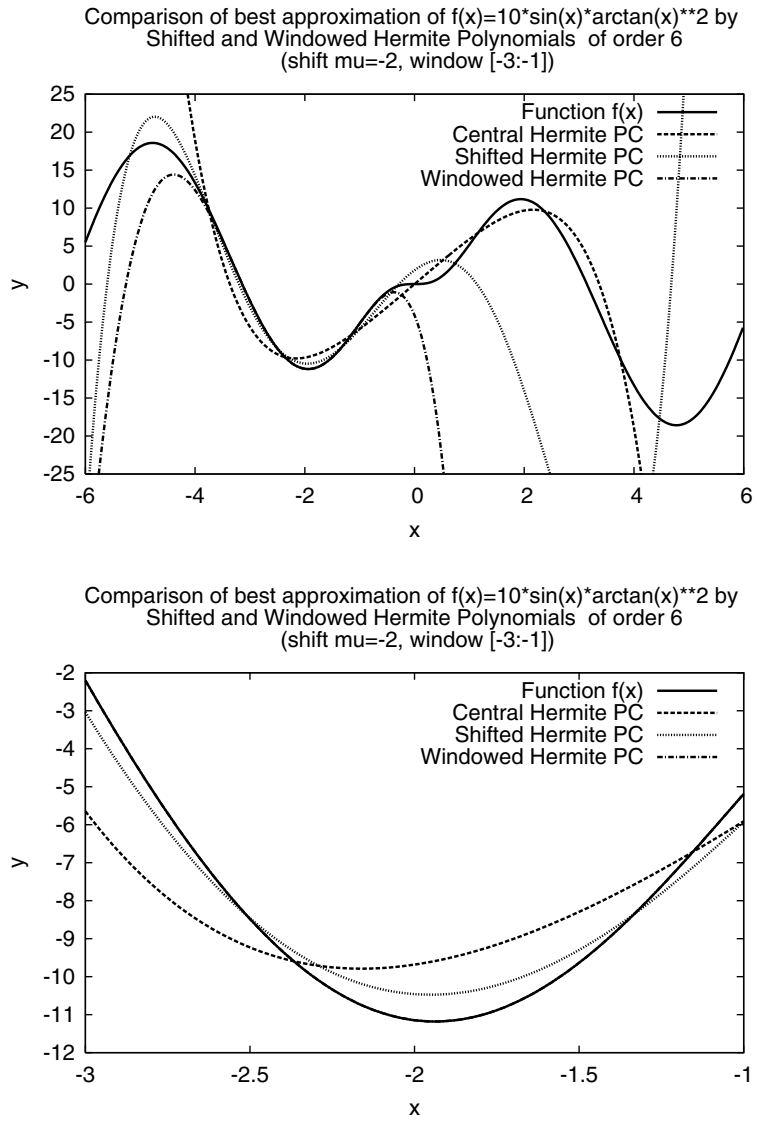

Fig. 4. Best approximation of the function $f(x) = 10 * \sin(x) * \arctan(x) ** 2$ in the range $[-6:6]$ (upper picture) and $[-4:-1]$ (lower picture) by shifted and windowed Hermite polynomials. It holds $\mu = -2$ for the shifted Hermite polynomials and $[a,b] = [-3,-1]$ for the windowed Hermite polynomials.

$$P(g(\boldsymbol{\xi}) \leqslant 0) = \int_{g(\boldsymbol{\xi}) \leqslant 0} \rho_{\boldsymbol{\xi}}(\boldsymbol{\xi})\, \mathrm{d}\boldsymbol{\xi} \tag{34}$$

$$= \int_{\mathbb{R}^n} \Gamma_g(\boldsymbol{\xi}) \rho_{\boldsymbol{\xi}}(\boldsymbol{\xi})\, \mathrm{d}\boldsymbol{\xi} \tag{35}$$

$$\approx \int_{\mathbb{R}^n} \Gamma_g^m(\boldsymbol{\xi}) \rho_{\boldsymbol{\xi}}(\boldsymbol{\xi})\, \mathrm{d}\boldsymbol{\xi}, \quad m = s, w \tag{36}$$

where

$$\Gamma_g(\boldsymbol{\xi}) = \begin{cases} 0 & \text{if } g(\boldsymbol{\xi}) > 0, \\ 1 & \text{if } g(\boldsymbol{\xi}) \leqslant 0, \end{cases} \quad \Gamma_g^m(\boldsymbol{\xi}) = \begin{cases} 0 & \text{if } g^m(\boldsymbol{\xi}) > 0, \\ 1 & \text{if } g^m(\boldsymbol{\xi}) \leqslant 0, \end{cases} \quad m = s, w. \tag{37}$$

The failure integral (36) can be computed, for example, by utilizing importance sampling on the Hermite approximation, see [14].

6. Applications

The performance of the methods is demonstrated on two applications which are based on ordinary differential equations. The differential equations which depend on the random variables are projected onto the Polynomial Chaos space by Galerkin's method as in (17). In the following, the term "shift" is used for the shift of method (SH) as well as for the center of the window of method (WH). For all examples, a fixed window size of $[\mu_1 - 2, \mu_1 + 2] \times \cdots \times [\mu_n - 2, \mu_n + 2]$ is chosen. Also, the order of Hermite approximation is always equal to 3. Standard, that means non-adaptive Gauss–Hermite quadrature has been applied for evaluation of the PC coefficients. The number s in (14) is 4, and the number of integration points N is 4 in the 1D and 64 in the 3D case, respectively.

6.1. The predator–prey model

Predator–prey dynamics can be described by the Lotka–Volterra model with two differential equations (see for example [21,20]):

$$\begin{aligned} \dot{x}(t) &= ax(t) - bx(t)y(t), \\ \dot{y}(t) &= bx(t)y(t) - cy(t). \end{aligned} \tag{38}$$

The prey population $x(t)$ increases by feeding and decreases by being fed by the predator. The predator population $y(t)$ increases by feeding and decreases by natural extinction. The rates a, b and c are assumed to be Gaussian random variables:

$$a(\Theta) = \bar{a} + \sigma_a \xi(\Theta), \tag{39}$$

$$b(\Theta) = \bar{b} + \sigma_b \xi(\Theta), \tag{40}$$

$$c(\Theta) = \bar{c} + \sigma_c \xi(\Theta). \tag{41}$$

Because there are three independent stochastic input variables, a three-dimensional polynomial expansion must be performed for the stochastic processes $x(t,\Theta)$ and $y(t,\Theta)$:

$$\begin{aligned} x(t,\Theta) &= X_0(t)\Psi_0(\Theta) + \sum_{i=1}^{3} X_i(t)\Psi_1(\xi_i(\Theta)) + \sum_{i=1}^{3}\sum_{j=1}^{i} X_{i,j}(t)\Psi_2\big(\xi_i(\Theta),\xi_j(\Theta)\big) \\ &\quad + \sum_{i=1}^{3}\sum_{j=1}^{i}\sum_{k=1}^{j} X_{i,j,k}(t)\Psi_3\big(\xi_i(\Theta),\xi_j(\Theta),\xi_k(\Theta)\big) + \cdots \\ y(t,\Theta) &= Y_0(t)\Psi_0(\Theta) + \sum_{i=1}^{3} Y_i(t)\Psi_1(\xi_i(\Theta)) + \sum_{i=1}^{3}\sum_{j=1}^{i} Y_{i,j}(t)\Psi_2(\xi_i(\Theta),\xi_j(\Theta)) \\ &\quad + \sum_{i=1}^{3}\sum_{j=1}^{i}\sum_{k=1}^{j} Y_{i,j,k}(t)\Psi_3(\xi_i(\Theta),\xi_j(\Theta),\xi_k(\Theta)) + \cdots \end{aligned} \tag{43}$$

where $\Psi_n(\xi_1,\ldots,\xi_n)$ may be central, shifted or windowed Hermite polynomials. Inserting the three-dimensional Hermite expansion into Eqs. (38) and testing the equations by the base functions gives the final probabilistic equations.

6.1.1. Results for the predator–prey model

In the one-dimensional test case, coefficients a and c in (38) are chosen as deterministic variables ($a = c = 0.1$) and coefficient b as a Gaussian random variable with mean 1.0 and standard deviation 0.1. For each time t, the failure probability is defined as the probability that the prey population $x(t,\Theta)$ becomes less than the bound $\epsilon = 1.\mathrm{e} - 6$:

$$g(x(t,\Theta)) = x(t,\Theta) - \epsilon.$$

Fig. 5 shows results for the exact solution, centered (CH), shifted (SH) and windowed Hermite (WH). The shift is $\mu = 4$ and the window $[2, 6]$. The failure probabilities for the exact solution are computed by sampling the integrand (the exact solution) in (34), the failure probabilities for (CH), (SH) and (WH) are computed by sampling the integrand (the Hermite approximation) in (36). For the exact solution and method (CH), Monte Carlo sampling is utilized, for (SH) and (WH) importance sampling. The number of Monte Carlo samples is very high (5,000,000) in order to resolve also very small failure probabilities. Table 1 shows the number of time steps, function and Hermite evaluations for this example. The number of Hermite evaluations is equal to the number of time steps times the number of Monte Carlo samples. It is evident from the table that crude Monte Carlo sampling is not competitive at all. For this example we have used the standard Gauss–Hermite quadrature. With the adaptive Gauss quadrature described in [7], a further reduction of function evaluations may be achieved for the Hermite methods. In addition, the last column of the table shows the number of function evaluations required for exact computation of the Beta point at a particular time point $t = 7$. This is included for comparison of the cost of computing approximate failure probabilities over a time range, on the one hand, and computing the failure probability using the FORM method at a certain time point, on the other hand. But note that exact computation of the Beta point has not been utilized for computing the results shown in Fig. 5.

Only for failure probabilities larger than 10^{-1}, (CH) gives acceptable results. Both (SH) and (WH) are much better than (CH) for small failure probabilities. For failure probabilities larger than 10^{-2} at time about 9.2, the (WH) curve is departing from the exact solution curve, because the critical failure region is leaving the window. So (SH) and (WH), with a given shift, can only resolve the exact solution curve in a time range where the Beta point does not move too far away from the shift. During sampling of the integrand in (36), an approximation of the Beta point may be computed by solving a discrete version of (20). Fig. 6 shows the transient evolution of the approximated Beta point and the distance to the shift for method (WH). Again this figure

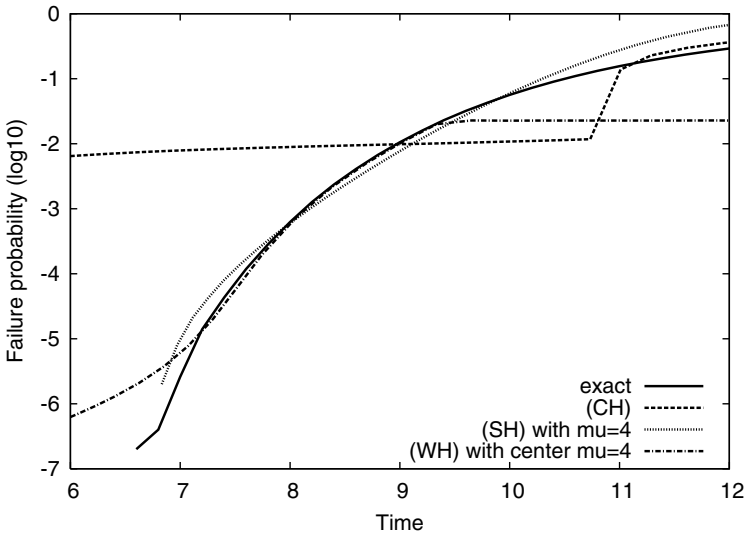

Fig. 5. Predator–prey model with a one-dimensional random vector: A comparison of failure probabilities for the exact solution (solid), centered Hermite (dashed), shifted Hermite (dotted) and windowed Hermite (dashed-dotted) for shift $\mu = 4$ and window $[2, 6]$.

Table 1
Predator–prey model with a one-dimensional random vector: number of time steps, function and Hermite calls for shift $\mu = 4$

	MC	CH	SH	WH	Beta ($t = 7$)
F-calls	1,759,798,365	1192	1172	1172	20,409
H-calls	–	680,000,000	675,000,000	695,000,000	–
Time steps	–	136	135	139	–

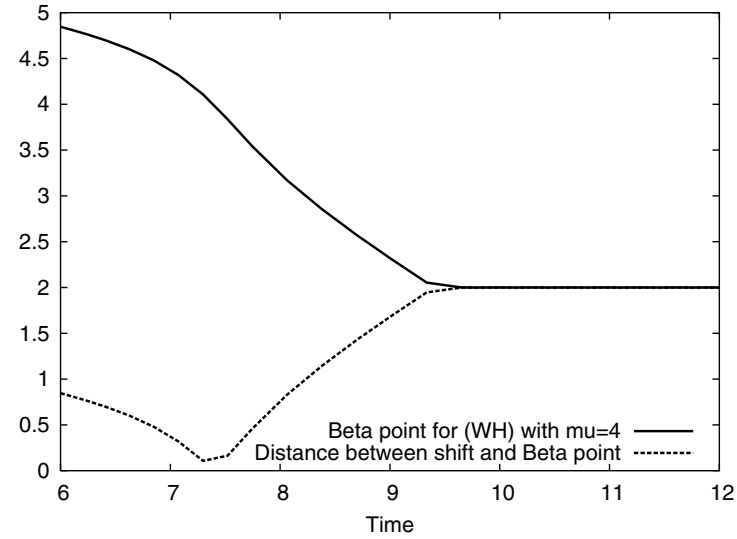

Fig. 6. Predator–prey model with a one-dimensional random vector: Approximated Beta point (solid) and distance between shift and Beta point (dashed) for method (WH) and window $[2,6]$.

reveals that the relevant time range for (WH) with shift $\mu = 4$ has an upper limit of about $t = 9.2$ because then the Beta point approaches the lower limit 2 of the window. For a better resolution of small failure probabilities, a larger shift is necessary. Fig. 7 shows a comparison for the shift $\mu = 5$ and the window $[3,7]$. Both the resolution of (SH) and (WH) of small failure probabilities is better than for $\mu = 4$, but the (WH) curve is departing from the exact solution curve for failure probabilities larger than 10^{-3}. Fig. 8 shows a comparison for the shift $\mu = 3$ and the window $[1,5]$. As this example shows, for problems with strongly changing failure probabilities, it would perhaps be better to adapt the shift with time.

In the three-dimensional test case, all coefficients a, b, c in (38) are chosen as Gaussian random variables, a and c with mean 0.1 and standard deviation 0.01, b with mean 1.0 and standard deviation 0.1. As initial guess, the shift for methods (SH) and (WH) is chosen as $(0,5,0)$, that means no shift for parameters a and b, and shift 5 for parameter b, which has turned out to be appropriate for small failure probabilities in the 1D case. Fig. 9

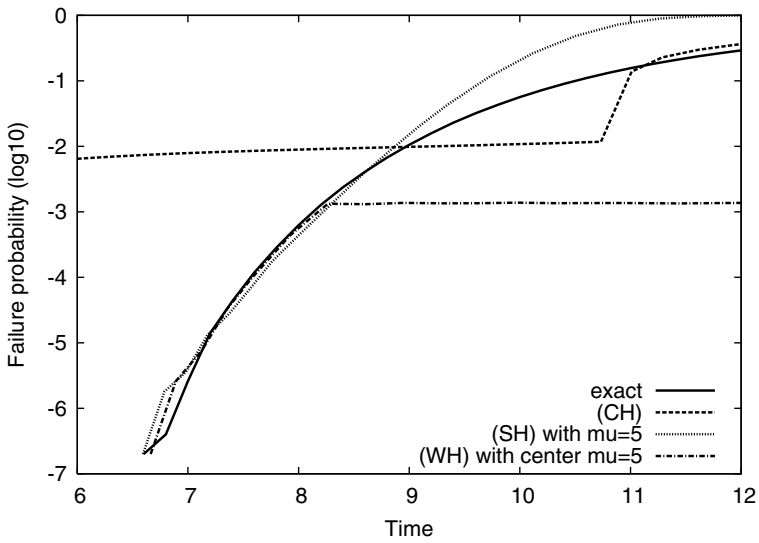

Fig. 7. Predator–prey model with a one-dimensional random vector: A comparison of failure probabilities for the exact solution (solid), centered Hermite (dashed), shifted Hermite (dotted) and windowed Hermite (dashed-dotted) for shift $\mu = 5$ and window $[3,7]$.

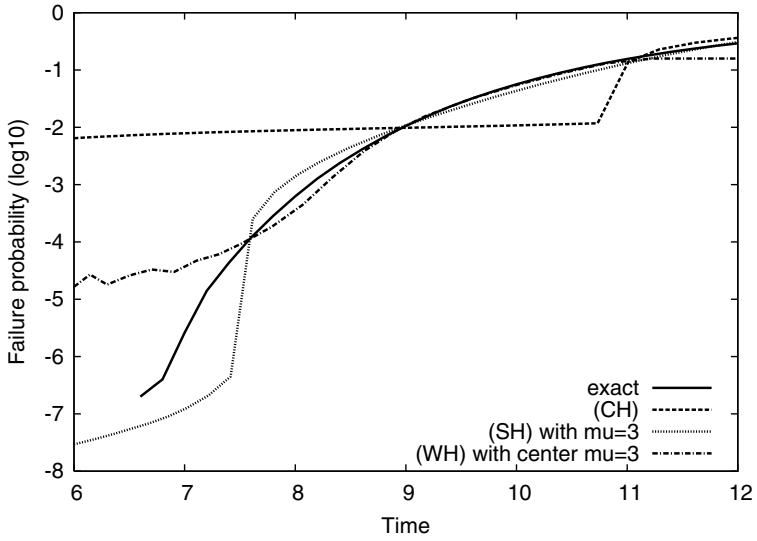

Fig. 8. Predator–prey model with a one-dimensional random vector: A comparison of failure probabilities for the exact solution (solid), centered Hermite (dashed), shifted Hermite (dotted) and windowed Hermite (dashed-dotted) for shift $\mu = 3$ and window $[1, 5]$.

shows results for the exact solution, centered, shifted and windowed Hermite. Table 2 shows the number of time steps, function and Hermite evaluations for this example. As in the 1D case, crude Monte Carlo sampling is not competitive at all. In addition, the last column of the table shows the number of function evaluations required for exact computation of the Beta point at a particular time point $t = 7$.

As can be seen in Fig. 9, (CH) only produces acceptable results for large failure probabilities. For small probabilities, (SH) and (WH) are much better, even for this coarse initial guess of the shift. As in the 1D case, the temporal evolution of the Beta point can be computed (see Fig. 10). The computed results of (WH) can only be trusted until $t = 8$, when the Beta point approaches the boundary of the window. This corresponds to the results in Fig. 9 where the (WH) curve is departing from the exact curve at $t = 8$. Again it may be better to dynamically adapt the shift to the computed Beta point. This will be investigated in the future. Here we restrict

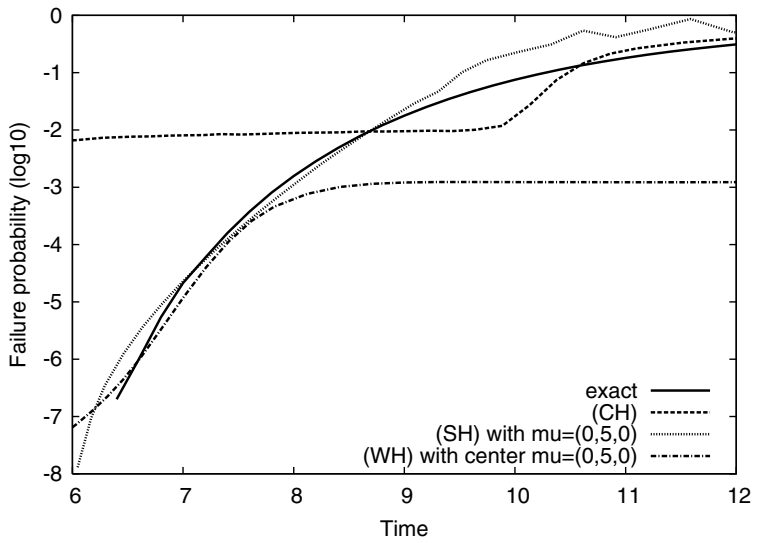

Fig. 9. Predator–prey model with a three-dimensional random vector: A comparison of failure probabilities for the exact solution (solid), centered Hermite (dashed), shifted Hermite (dotted) and windowed Hermite (dashed-dotted) with shift $(0, 5, 0)$.

Table 2
Predator–prey model with a three-dimensional random vector: number of time steps, function and Hermite calls for shift $(0,5,0)$

	MC	CH	SH	WH	Beta ($t=7$)
F-calls	1,765,566,892	53,814	60,096	55,424	18,342
H-calls	–	840,000,000	905,000,000	780,000,000	–
Time steps	–	168	181	156	–

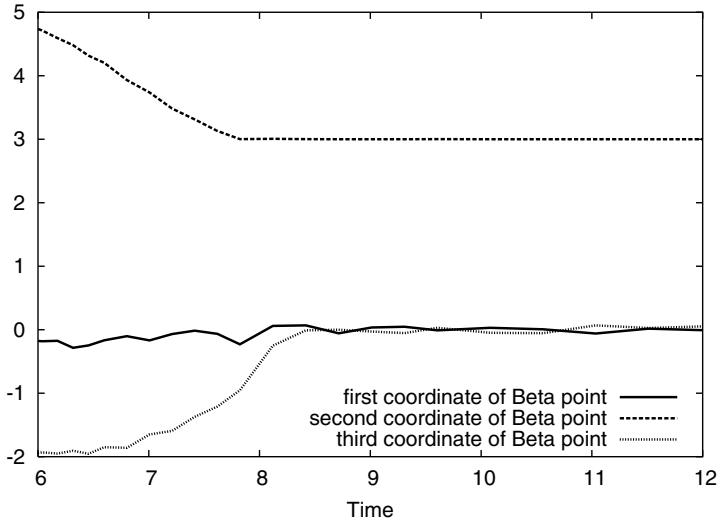

Fig. 10. Predator–prey model with a three-dimensional random vector: Approximated coordinates of Beta point computed by method (WH) and center $(0,5,0)$.

ourselves to fixed shift computations. Fig. 10 shows approximate Beta points $(0,5,-2)$, $(0,4,-2)$ and $(0,3,-1)$ for times $t=6$, $t=7$ and $t=8$, respectively. Using these vectors as shifts for (SH) and (WH), one may resolve different time ranges and failure probabilities.

6.2. The Belousov–Zhabotinsky reaction

The Belousov–Zhabotinsky reaction is an example of an homogeneous oscillating system and can be described by the following set of ordinary differential equations (see [15])

$$\begin{aligned}
\frac{\mathrm{d}c(X)}{\mathrm{d}t} &= k_1 c(A)c(Y) + k_2 c(A)c(X) - k_3 c(X)c(Y) - 2k_4 c^2(X),\\
\frac{\mathrm{d}c(Y)}{\mathrm{d}t} &= -k_1 c(A)c(Y) - k_3 c(X)c(Y) + \frac{f}{2} k_5 c(B)c(Z),\\
\frac{\mathrm{d}c(Z)}{\mathrm{d}t} &= 2k_2 c(A)c(X) - k_5 c(B)c(Z).
\end{aligned} \tag{44}$$

The notation is given in Table 3, the initial values are given in Table 4.

Fig. 11 shows the deterministic solution. For the stochastic computation, coefficient k_1 in (44) is assumed to be a Gaussian variable with mean 1.28 mol L^{-1} and standard deviation 0.064 (which corresponds to a coefficient of variation of 0.05). An artificial failure criterion is chosen being based upon the amplitude of the bromide ions curve. As one can see in deterministic computations, the amplitude gets smaller with increasing k_1. The 'failure' probability is now defined as the probability that the amplitude of the bromide ions curve is smaller than the bound $\epsilon = 9.\mathrm{e}-5$:

$$g(\Theta) = \max_t c(Y)(t,\Theta) - \epsilon. \tag{45}$$

Table 3
Legend of the Belousov–Zhabotinsky reaction

Variable	Substance
A	Bromate ions
B	Mixture of malonic and bromic acid
X	Bromic acid
Y	Bromide ions
Z	Manganese(III) ions

Table 4
Initial values of the Belousov–Zhabotinsky reaction

Variable	Value
A	0.06 mol L^{-1}
B	0.02 mol L^{-1}
X	2.e − 7 mol L^{-1}
Y	2.e − 5 mol L^{-1}
Z	1.e − 4 mol L^{-1}
k_1	1.28 L mol^{-1} s^{-1}
k_2	8 L mol^{-1} s^{-1}
k_3	8.e5 L mol^{-1} s^{-1}
k_4	2.e3 L mol^{-1} s^{-1}
k_5	1 L mol^{-1} s^{-1}
f	1.5

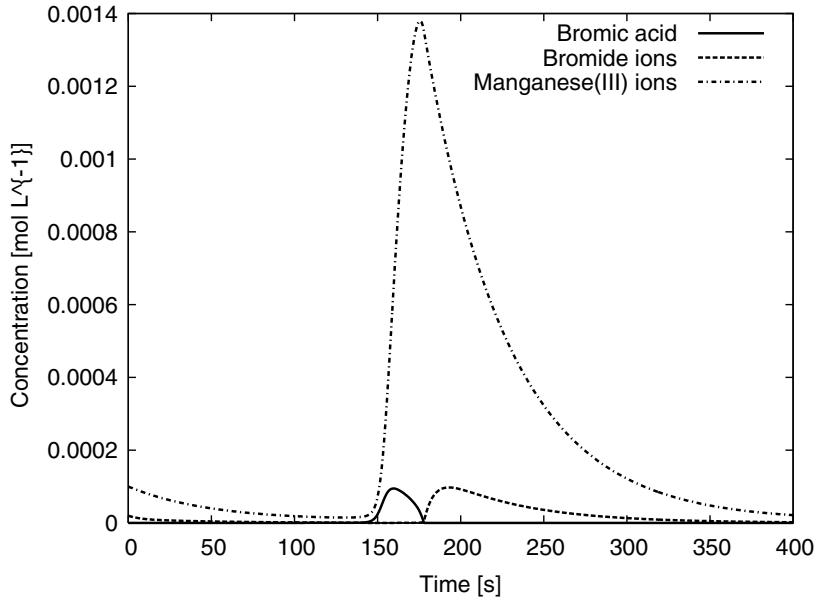

Fig. 11. Deterministic solution of the Belousov–Zhabotinsky reaction.

In this example, the failure function g is not time dependent. Failure functions of type (45) can generally be used in problems where one asks for the probability of oscillations. The computed failure probabilities are shown in Table 5. Method (CH) does not detect failure at all. Method (WH) shows the best approximations. In this example, (SH) does not give satisfactory results. In all examples we have chosen a fixed variance for (SH). Additional tests have shown that (SH) with smaller variance lead to comparable results as (WH). The choice of the optimal window size of (WH) and the variance of (SH) will be the subject of future investigations.

Table 5
Computed failure probabilities for the Belousov–Zhabotinsky reaction

Method	Failure probability
Exact solution	0.0186
(CH)	0.0
(SH) with shift 2	0.0082
(SH) with shift 3	0.0145
(SH) with shift 4	0.047
(WH) with window [0,4]	0.0177
(WH) with window [1,5]	0.0183
(WH) with window [2,6]	0.0203

7. Conclusion

Polynomial chaos expansion may be interpreted as a perturbation ansatz of a stochastic process about its mean. In this paper, we have considered two methods of adapting polynomial chaos expansion to failure detection. Here, the mean is no longer of interest, but the tail of the stochastic distribution.

In the examples presented, (SH) and (WH) showed satisfactory results.

Both proposed methods depend on a good estimation of the shift μ. The usual procedure is to determine the point of largest probability of failure, see Eq. (20). For ordinary differential equations, this optimal shift may be determined once for the initial values. The time evolution of the Beta point/shift is then given by the Kuhn–Tucker equations

$$\begin{aligned} &g(\mathbf{x}(\mu_1,\cdots\mu_n,\mathbf{t}))=0,\\ &2\mu_i+\lambda\sum_{k=1}^{n}\frac{\partial_g(\mathbf{x}(\mu_1,\ldots,\mu_n,\mathbf{t}))}{\partial x_k}\frac{\partial x_k}{\partial \mu_i}=0,\quad i=1,\ldots,n \end{aligned} \tag{46}$$

which may be coupled with the PC system. The resulting system is a differential algebraic system which must be solved by implicit integration methods. Another possibility is to integrate the time derivative of Eq. (46) in combination with the PC system.

Both methods have been applied to two examples which are based on ordinary differential equations. The methods are also suitable for other models such as stochastic finite elements. Here, the optimization problem (20) of finding the point with largest probability of failure is also solved once. The element with the largest stress defines the failure function with a corresponding Beta point and shift. With this shift or window, a polynomial chaos expansion may be performed.

In this paper, we have demonstrated the benefit of shifted and windowed polynomial chaos expansions for failure detection. Further work will be spent on achieving efficient and accurate methods for the determination and the adaption of the optimal shift/window.

Acknowledgement

The authors are indebted to Prof. A. Gilg's analysis group for many valuable discussions.

Appendix A. Gram–Schmidt orthogonalization procedure for windowed Hermite polynomials

(1) Initialize:

$$\begin{aligned} &\tilde{\phi}_0(x)=1,\\ &c^0=\left\|\tilde{\phi}_0(x)\right\|_w,\\ &\phi_0(x)=1/c^0. \end{aligned}$$

(2) For $k = 0, \ldots, n$:

$$\tilde{\phi}_{k+1}(x) = \left(\frac{x-\mu}{b-a}\right)^{k+1} - \sum_{j=0}^{k} a_j^{k+1}\phi_j(x),$$
$$a_j^{k+1} = \left\langle \left(\frac{x-\mu}{b-a}\right)^{k+1}, \phi_j(x) \right\rangle_w, \quad j = 0, \ldots, k,$$
$$c^{k+1} = \left\| \tilde{\phi}_{k+1}(x) \right\|_w,$$
$$\phi_{k+1}(x) = \sum_{i=0}^{k+1} b_i^{k+1} \left(\frac{x-\mu}{b-a}\right)^i,$$
$$b_i^{k+1} = \sum_{j=i}^{k} a_j^{k+1} b_i^j / c^{k+1}, \quad i = 0, \ldots, k,$$
$$b_{k+1}^{k+1} = 1/c^{k+1}.$$

Appendix B. Error estimation of windowed Hermite chaos

In practical applications, one will either combine windowed Hermite chaos with shifted Hermite chaos or use multiple windowed Hermite chaos with two windows, a smaller and a larger one. This section, in contrast, deals with error estimation of single windowed Hermite chaos applied for computation of failure integrals. The analysis is performed for a rotated window W_{rot}, and all functions are formulated in the rotated coordinate system, with the last coordinate along the direction of $-\nabla_g(\boldsymbol{\xi})$ in the Beta point, see Fig. B.1. Let $\tilde{H}(\boldsymbol{\eta})$ the Hermite approximation of $\tilde{g}(\boldsymbol{\eta})$ in the rotated coordinate system, $a_i \leqslant \eta_i \leqslant b_i,\ i = 1, \ldots, n$. Then the failure integral

$$P_{\text{f}} = \int_{\tilde{g}(\boldsymbol{\eta}) \leqslant 0} \tilde{\rho}(\boldsymbol{\eta})\, \mathrm{d}\boldsymbol{\eta}$$

is approximated by

$$\tilde{P}_{\text{f}} = \int_{\tilde{H}(\boldsymbol{\eta}) \leqslant 0, \boldsymbol{\eta} \in W_{\text{rot}}} \tilde{\rho}(\boldsymbol{\eta})\, \mathrm{d}\boldsymbol{\eta}.$$

The error $E_{\text{f}} = P_{\text{f}} - \tilde{P}_{\text{f}}$ consists of two components, the error $E_{\text{f}}^{(1)}$ inside and the error $E_{\text{f}}^{(2)}$ outside the window:

$$E_{\text{f}} = \underbrace{\left[\int_{\tilde{g}(\boldsymbol{\eta}) \leqslant 0, \boldsymbol{\eta} \in W_{\text{rot}}} \tilde{\rho}(\boldsymbol{\eta})\, \mathrm{d}\boldsymbol{\eta} - \int_{\tilde{H}(\boldsymbol{\eta}) < 0, \boldsymbol{\eta} \in W_{\text{rot}}} \tilde{\rho}(\boldsymbol{\eta})\, \mathrm{d}\boldsymbol{\eta} \right]}_{E_{\text{f}}^{(1)}} + \underbrace{\int_{\tilde{g}(\boldsymbol{\eta}) \leqslant 0, \boldsymbol{\eta} \notin W_{\text{rot}}} \tilde{\rho}(\boldsymbol{\eta}) d\boldsymbol{\eta}}_{E_{\text{f}}^{(2)}}.$$

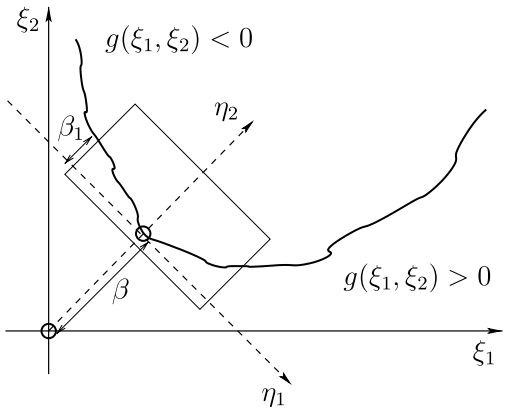

Fig. B.1. Error estimation of failure integral approximation by windowed Hermite.

As we will see is the error dependent on the slope and curvature of $\tilde{g}$ in zeroes of $\tilde{g}$. The larger the slope and curvature, the smaller will be the error.

B.1. Error estimation of $E_{\mathrm{f}}^{(I)}$

For error estimation of $E_{\mathrm{f}}^{(1)}$, we will assume that the following two conditions are fulfilled:

- $\tilde{H}(\boldsymbol{\eta})$ approximates $\tilde{g}(\boldsymbol{\eta})$ uniformly in W_{rot}, i.e. $\exists \delta > 0$ with
$$|\tilde{g}(\boldsymbol{\eta}) - \tilde{H}(\boldsymbol{\eta})| \leqslant \delta \quad \forall \boldsymbol{\eta} \in W_{\mathrm{rot}}. \tag{B.1}$$
- The slope of $\tilde{g}$ in the neighbourhood of zeroes of $\tilde{g}$ must be sufficiently large, more precisely, for $0 < \beta < B$ exist $0 < \alpha_0 < \alpha_1$ with
$$\begin{aligned} &\tilde{g}(\eta_1^0, \ldots, \eta_{n-1}^0, \eta_n^0 + \alpha) < -\beta, \\ &\tilde{g}(\eta_1^0, \ldots, \eta_{n-1}^0, \eta_n^0 - \alpha) > \beta \end{aligned} \tag{B.2}$$

for all zeroes $\boldsymbol{\eta}^0 \in W_{\mathrm{rot}}$ of $\tilde{g}$ and $\alpha_0 \leqslant \alpha \leqslant \alpha_1$.

Additionally, it is assumed that

$$S := \{\boldsymbol{\eta} | \tilde{g}(\boldsymbol{\eta}) \leqslant 0\} \text{ is convex.} \tag{B.3}$$

Define

$$\begin{aligned} N_g(\eta_1, \ldots, \eta_{n-1}) &= \{\eta_n | \tilde{g}(\eta_1, \ldots, \eta_n) \leqslant 0, a_n \leqslant \eta_n \leqslant b_n\}, \\ N_H(\eta_1, \ldots, \eta_{n-1}) &= \{\eta_n | \tilde{H}(\eta_1, \ldots, \eta_n) \leqslant 0, a_n \leqslant \eta_n \leqslant b_n\} \end{aligned}$$

and

$$g_N(\eta_1, \ldots, \eta_{n-1}) = \begin{cases} \min\limits_{\eta_n} N_g(\eta_1, \ldots, \eta_{n-1}) & \text{if } N_g(\eta_1, \ldots, \eta_{n-1}) \neq \emptyset, \\ b_n & \text{else,} \end{cases}$$

$$H_N(\eta_1, \ldots, \eta_{n-1}) = \begin{cases} \min\limits_{\eta_n} N_H(\eta_1, \ldots, \eta_{n-1}) & \text{if } N_H(\eta_1, \ldots, \eta_{n-1}) \neq \emptyset, \\ b_n & \text{else.} \end{cases}$$

Now choose $\beta = \delta$ in (B.2), with δ from (B.1). This is always possible if $B > \delta$. From (B.1), (B.2) it follows that:

$$\max_{\eta_1, \ldots, \eta_{n-1}} |g_N(\eta_1, \ldots, \eta_{n-1}) - H_N(\eta_1, \ldots, \eta_{n-1})| \leqslant \alpha_0. \tag{B.4}$$

Then

$$\begin{aligned} |E_{\mathrm{f}}^{(1)}| &= \Big| \int_{a_1}^{b_1} \cdots \int_{a_{n_1}}^{b_{n-1}} \int_{g_N(\eta_1, \ldots, \eta_{n-1})}^{b_n} \tilde{\rho}(\boldsymbol{\eta}) \, \mathrm{d}\eta_n \ldots \mathrm{d}\eta_1 - \int_{a_1}^{b_1} \cdots \int_{a_{n-1}}^{b_{n-1}} \int_{H_N(\eta_1, \ldots, \eta_{n-1})}^{b_n} \tilde{\rho}(\boldsymbol{\eta}) \, \mathrm{d}\eta_n \ldots \, \mathrm{d}\eta_1 \Big| \\ &\leqslant \int_{a_1}^{b_1} \cdots \int_{a_{n-1}}^{b_{n-1}} |g_N(\eta_1, \ldots, \eta_{n-1}) - H_N(\eta_1, \ldots, \eta_{n-1})| \max_{\eta n} \tilde{\rho}(\boldsymbol{\eta}) \, \mathrm{d}\eta_{n-1} \ldots \, \mathrm{d}\eta_1 \\ &\leqslant \prod_{i=1}^{n-1} (b_i - a_i) \max_{\eta_1, \ldots, \eta_{n-1}} |g_N(\eta_1, \ldots, \eta_{n-1}) - H_N(\eta_1, \ldots, \eta_{n-1})| \max_{\boldsymbol{\eta} \in W_{\mathrm{rot}}} \tilde{\rho}(\boldsymbol{\eta}) \leqslant \prod_{i=1}^{n-1} (b_i - a_i) \alpha_0 \max_{\boldsymbol{\eta} \in W_{\mathrm{rot}}} \tilde{\rho}(\boldsymbol{\eta}). \end{aligned}$$

So, the larger the slope of $\tilde{g}$ in the neighbourhood of zeroes, the smaller will be α_0 and the error $E_{\mathrm{f}}^{(1)}$.

B.2. Error estimation of $E_{\mathrm{f}}^{(2)}$

Consider the optimization problem

$$\begin{aligned} &\min \quad \eta_n \\ &\text{w.r.t.} \quad \tilde{g}(\boldsymbol{\eta}) \leqslant 0, \quad \boldsymbol{\eta} \notin W_{\mathrm{rot}} \end{aligned} \tag{B.5}$$

The minimum $\boldsymbol{\eta}^{\min}$ of (B.5) is located at the boundary $\partial W_{\mathrm{rot}}$ of W_{rot}.

Proof. Let $\boldsymbol{\eta}^{\min} \notin \overline{W_{\text{rot}}}$. Connect $\boldsymbol{\eta}^{\min}$ with 0 (the Beta point). From (B.3) it follows that, for all points on this line, it holds $\tilde{g}(\boldsymbol{\eta}) \leqslant 0$. The line must cut ∂W_{rot} in a point $\boldsymbol{\eta}^{w}$. On the other hand, the coordinate η_n decreases monotonically along the line. So $\eta_m^W < \eta_n^{\min}$ which is a contradiction. □

It follows that all $\boldsymbol{\eta}$, for which $\tilde{g}(\boldsymbol{\eta}) \leqslant 0$ and $\boldsymbol{\eta} \notin W_{\text{rot}}$, lie in the half plane $P = \{\boldsymbol{\eta} \| \eta_n \geqslant \eta_n^{\min} \geqslant 0\}$. Analogously to the FORM ansatz it holds

$$\int_{\boldsymbol{\eta} \in P} \tilde{\rho}(\boldsymbol{\eta})\, \mathrm{d}\boldsymbol{\eta} = \Phi(-\beta - \eta_n^{\min}) \tag{B.6}$$

with Φ denoting the cumulative density function of the standard 1D normal distribution. So

$$\left\| E_{\text{f}}^{(2)} \right\| \leqslant \int_{\boldsymbol{\eta} \in P} \tilde{\rho}(\boldsymbol{\eta})\, \mathrm{d}\boldsymbol{\eta} = \Phi\left(-\beta - \eta_n^{\min}\right). \tag{B.7}$$

See also Fig. B.1 where $\eta_n^{\min}$ is denoted by β_1. So, the larger the curvature of $\tilde{g}$ in the Beta point, the larger will be $\eta_n^{\min}$ and the smaller the error $E_{\text{f}}^{(2)}$.

References

[1] K.W. Breitung, Asymptotic approximations for probability integrals, Lecture Notes in Mathematics 1592, Springer, Berlin, 1994.
[2] R. Cameron, W. Martin, The orthogonal development of nonlinear functional in series of Fourier–Hermite functionals, Ann. Math. 48 (2) (1947) 385–392.
[3] Philip J. Davis, Methods of Numerical Integration (Computer Science and Applied Mathematics), Academic Press, New York, 1975.
[4] R. Ghanem, P.D. Spanos, Stochastic Finite Elements – A Spectral Approach, Springer, Berlin, 1991.
[5] R. Ghanem, Hybrid stochastic finite elements and generalized Monte Carlo simulation, Trans. ASME 65 (1998) 1004–1009.
[6] R. Ghanem, Ingredients for a general purpose stochastic finite elements implementation, Comput. Methods Appl. Mech. Eng. 168 (1999) 19–32.
[7] M. Herzog, A. Gilg, M. Paffrath, P. Rentrop, U. Wever, Intrusive versus non-intrusive methods for stochastic finite elements, in: M. Breitner, E. Denk, P. Rentrop (Eds.), From Nano to Space, Applied Mathematics inspired by R. Bulirsch, Springer, Berlin, 2007.
[8] M. Hohenbichler, R. Rackwitz, First-order concepts in system reliability, Struct. Safety 1 (1983) 177–188.
[9] M. Hohenbichler, S. Gollwitzer, W. Kruse, R. Rackwitz, New light on first- and second-order reliability methods, Struct. Safety 4 (1987) 267–284.
[10] G.E. Karniadakis, C.H. Su, D. Xiu, D. Lucor, C. Schwab, R.A. Todor: Generalized polynomial chaos solution for differential equations with random inputs ETH Zürich, Research Report No. 2005-01, 2005.
[11] A. Der Kiureghian, The geometry of random vibrations and solutions by FORM and SORM, Probab. Eng. Mech. 15 (2000) 81–90.
[12] O.P. LeMaitre, O.M. Knio, H.N. Najm, R.G. Ghanem, Uncertainty propagation using Wiener–Haar expansions, J. Comput. Phys. 197 (2004) 28–57.
[13] O.P. LeMaitre, H.N. Hajm, R.G. Ghanem, O.M. Knio, Multi-resolution analysis of Wiener-type uncertainty propagation schemes, J. Comput. Phys. 197 (2004) 502–531.
[14] R.E. Melchers, Structural Reliability Analysis and Prediction, Wiley, New York, 1999.
[15] I. Motoike, A. Adamtzky, Three-valued logic gates in reaction–diffusion excitable media, Solitons & Fractals 24 (2005) 107–114.
[16] H.J. Pradtlwarter, G.I. Schuëller, On advanced Monte Carlo simulation procedures in stochastic structural dynamics, Int. J. Non-Linear Mech. 32 (4) (1997) 735–744.
[17] R. Rackwitz, Reliability analysis – a review and some perspectives, Struct. Safety 23 (2001) 365–395.
[18] M. Rosenblatt, Remarks on a multivariate transformation, Ann. Math. Stat. 23 (1952) 470–472.
[19] M. Schevenels, G. Lombaert, G. Degrande, Application of the stochastic finite element method for Gaussian and non-Gaussian systems, in: Proceedings of ISMA, 2004.
[20] R.J. Swift, A stochastic predator–prey model, Irish Math. Soc. Bull. 48 (2002) 57–63.
[21] V. Volterra, Variations and fluctuations of the number of individuals in animal species living together, in: Animal Ecology, McGraw-Hill, New York, 1931.
[22] J. Stoer, R. Bulirsch, Introduction to Numerical Analysis, Springer, New York, 1980.
[23] X. Wan, G.E. Karniadakis, An adaptive multi-element generalized polynomial chaos method for stochastic differential equations, J. Comput. Phys. 209 (2005) 617–642.
[24] X. Wan, G.E. Karniadakis, Multi-element generalized polynomial chaos for arbitrary probability measures, SIAM J. Sci. Comput. 28 (3) (2006) 901–928.
[25] N. Wiener, The homogeneous chaos, Am. J. Math. 60 (1938) 897–936.
[26] D. Xiu, G.E. Karniadakis, The Wiener–Askey polynomial chaos for stochastic differential equations, SIAM J. Sci. Comput. 24 (2) (2002) 619–644.